ORIGINAL RESEARCH

Hollow carbon microspheres modified with $NiCo_2S_4$ nanosheets as a high-performance microwave absorber

Peitao Hu[1] · Shun Dong[1] · Fang Yuan[2] · Xiutao Li[3] · Changqing Hong[1]

Abstract

Due to the unique advantages including low density, good chemical stability, and superior dielectric property, carbon-based materials have been exploited as potential microwave absorbers and have become a research hotspot. Herein, a superior microwave absorbent consisting of $NiCo_2S_4$ nanosheets anchored on hollow carbon spheres is successfully designed and fabricated by a low-cost and facile strategy for the first time. The obtained $C/NiCo_2S_4$ composite shows a minimum reflection loss (RL_{min}) of −65.10 dB with a matching thickness of only 1.56 mm, and the effective absorption bandwidth (EAB) could reach up to 6.60 GHz at a thin thickness of 1.75 mm, which is a highly competitive carbon-based absorber. The existence of $NiCo_2S_4$ nanosheets balances the impedance matching property and enhances the dielectric loss effectively, and the cavity structure promotes the multiple reflections of the electromagnetic wave (EMW), which increases the energy loss capacity of the material. This study provides new insight into design and modification of hollow carbon spheres and broadens their application in the field of efficient microwave absorbers.

1 Introduction

The upgrades of the communication technology always bring huge social influences, and the developments of the 2G, 3G, and 4G technologies bring us text chat, image browsing, and video viewing, which greatly shorten the distance between people. In recent years, the rapid diffusion of 5G technology has promoted the developments of the virtual reality and smart home industry, which have significantly improved our living standards. However, the emergence of electromagnetic waves (EMWs) during this process has been

serious environmental pollution that influences the normal operation of sophisticated electronic equipment and threatens people's health [1–5]. To solve this problem, a large number of researchers have devoted themselves to exploring high-performance EMW-absorbing materials with a strong absorption capacity and a wide effective absorption bandwidth (EAB), and the relative field has been a research focus in recent years [6, 7].

Nowadays, several kinds of wave-absorbing materials have been prepared, and carbon-based materials attract researchers' much interest due to their several tremendous advantages including low density, good corrosion resistance, and superior dielectric property [8, 9]. After years of effort, researchers have studied the properties of carbonaceous absorbing materials with different structures, such as graphene [10, 11], carbon fibers [12, 13], carbon nanotubes [14], and carbon spheres [15, 16]. However, due to the single dielectric loss, carbonaceous materials often suffered from an impedance mismatch, and the reflection loss (RL) of the single material is generally weaker than −30.00 dB; using carbonaceous material to fabricate wave absorbers with strong absorption, a wide bandwidth, and a thin matching thickness still faces great challenges [17]. Concerning this problem, researchers have presented an

Peitao Hu and Shun Dong contributed equally to this work.

✉ Shun Dong
dongshun@hit.edu.cn

1 National Key Laboratory of Science and Technology for National Defence on Advanced Composites in Special Environments, Harbin Institute of Technology, Harbin 150001, People's Republic of China

2 Aerospace Research Institute of Materials & Processing Technology, Beijing 100076, People's Republic of China

3 China Academy of Launch Vehicle Technology, Beijing 100076, People's Republic of China

effective way of combining carbonaceous materials with other materials that could optimize the impedance matching of the samples, leading to a better absorption performance. For example, Qiu et al. fabricated hollow Ni/C microspheres utilizing Ni-MOF as the precursor, and the RL_{min} was up to −57.25 dB at 1.80 mm and its EAB could achieve 5.10 GHz [18]. Ning et al. modified hollow carbon microspheres with MoS_2 nanosheets, and the samples show an excellent absorption performance, whose RL_{min} could reach about −60.00 dB with a thickness of 2.00 mm [19].

Currently, as a binary sulfide, $NiCo_2S_4$ has been deeply studied in the field of electrochemistry [20–22]; exploring the microwave absorption performance of $NiCo_2S_4$ is of great significance to broaden its application field. Previous research has proved that $NiCo_2S_4$ possesses a certain absorbing capacity according to the previous literature [23]. Composing $NiCo_2S_4$ with carbon can effectively improve the absorbing property of the material, which is a potential research field [23, 24]. Zhao et al. fabricated r-GO/a-CNT/ $NiCo_2S_4$ composites, which showed a wonderful absorption performance [23], but these possessed the disadvantages of high cost. Dong et al. utilized biomass-derived carbon as templates, and $NiCo_2S_4$ nanosheets were used to modify the frameworks. The composites showed a superior absorption performance, and the minimum reflection loss could reach stronger than −60.00 dB; however, the composites faced a problem in which the uniformity of nanostructure distribution needs to be further improved [24]. Against this background, carbon microspheres with features of high yield and being easily wrapped result in a preparation process of uniform coating of the spheres that is simple and low cost, and thus, they are considered promising carbon templates [25, 26]. Meanwhile, lots of studies have reported that carbon spheres with a hollow structure may possess broader prospects than solid spheres on account of their hollow structure not only promoting multiple reflections of EMWs but also reducing the density of the material [27]. However, as far as we know, the research on the application of hollow carbon spheres modified by $NiCo_2S_4$ in the field of wave absorption is still blank.

Inspired by the above, in this work, we design and fabricate hollow carbon spheres decorated by a $NiCo_2S_4$ nanosheet structure through a subtle procedure. Firstly, we utilize SiO_2 microspheres as templates, using a low-cost method to fabricate carbon coating on SiO_2 and grow $NiCo_2S_4$ on the carbon shell. During this process, C/ $NiCo_2S_4$ with a hollow spherical structure is prepared by removing the SiO_2 core through a hydrolysis reaction. The introduction of $NiCo_2S_4$ and the existence of the spherical cavity effectively enhance the impedance matching and the attenuation constant of the material, and the RL_{min} of the composite reaches −65.10 dB with a matching thickness

of 1.56 mm and the EAB achieves up to 6.60 GHz, which covers the whole Ku band, exhibiting a superior absorption performance, which can act as a potential absorbent for utilizing in the next-generation wave-absorbing materials.

2 Experimental

2.1 Raw materials

Glucose ($C_6H_{12}O_6$), cobalt nitrate hexahydrate ($Co(NO_3)_2·6H_2O$), nickel nitrate hexahydrate ($Ni(NO_3)_2·6H_2O$), urea ($CO(NH_2)_2$), sodium sulfide nonahydrate ($Na_2S·9H_2O$), hydrochloric acid (HCl, 37%), hydrofluoric acid (HF, 25%), and deionized (DI) water were received from Harbin Kecheng Chemistry Company. Silica (SiO_2) powder was bought from Aladdin. All chemicals were directly used without further purification.

2.2 Synthesis of SiO_2@C

A SiO_2@C composite with a core@shell structure was successfully prepared via a hydrothermal treatment and calcination process. At first, 1.5 g glucose was dispersed into 30 mL DI water, and the mixture was stirred for 10 min to obtain a transparent solution, and then HCl was dropped into the solution until the pH = 1 to construct an enabling environment for the growth of carbon coating [28]. Subsequently, 0.3 g SiO_2 powder was put into the above solution and the mixture was transferred into a 50-mL Teflon-lined stainless steel autoclave and kept at 180 °C for 6 h; after cooling to room temperature naturally, the products were separated by centrifugation and dried at 70 °C for 24 h. Then, the samples were calcinated in a tube furnace at 1200 °C for 2 h under a flowing Ar atmosphere to obtain the SiO_2@C composite, and the heating rate and cooling rate were all 5 °C/min.

2.3 Synthesis of C/$NiCo_2S_4$

In a typical process, 1.5 mmol $Ni(NO_3)_2·6H_2O$, 3.0 mmol $Co(NO_3)_2·6H_2O$, and 7.5 mmol urea were dissolved into 30 mL DI water. Then, after stirring for 15 min, the obtained SiO_2@C composite was added to the dark red transparent solution and the mixture was totally poured into a 50-mL Teflon-lined stainless steel autoclave and heated at 120 °C for 6 h. After that, the products were centrifuged and dried at 70 °C for 24 h. Subsequently, the above samples were put into 30 mL 0.4 mol/L Na_2S solution and transferred to a 50-mL autoclave, kept at 180 °C for 6 h. Eventually, the C/$NiCo_2S_4$ composite was obtained after centrifugation,

Fig. 1 The schematic diagram of the synthesis process of C/NiCo$_2$S$_4$ composite
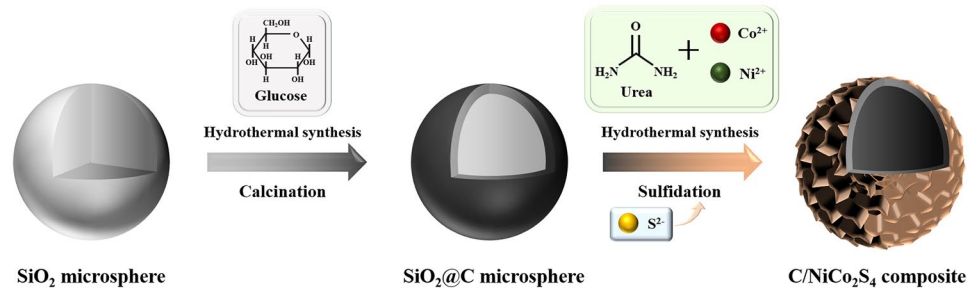
washed with DI water, and dried in an oven at 70 °C for 24 h.

2.4 Characterization

X-ray diffraction (XRD; X'PERT PRO MPD, Holland) was utilized to analyze the phase compositions of the samples with Cu Kα radiation of 40 kV. Raman spectra were collected by Raman microscopy (Renishaw, inVia) using a 633-nm laser. X-ray photoelectron spectroscopy (XPS; ESCALAB 250Xi, USA) was employed to comprehend the elemental states of the surface of the samples. The surface morphologies and the microstructures of the products were observed through scanning electron microscopy (SEM, HELIOS NanoLab 600i, USA) and transmission electron microscopy (TEM; Tecnai G^2-F30, USA) with energy-dispersive spectroscopy (EDS). The electromagnetic parameters of the materials were measured by a vector network analyzer (Agilent N5230A, USA) between 2 and 18 GHz, and the tested sample was uniformly mixed with 50 wt% paraffin followed by pressing into a coaxially shaped structure with $d_{out} = 7.00$ mm and $d_{in} = 3.04$ mm.

3 Results and discussion

The schematic diagram of the synthesis procedure of the C/NiCo$_2$S$_4$ composite is shown in Fig. 1, and the process is mainly divided into two links. Firstly, the carbon coating was prepared on the surface of SiO$_2$ microspheres through a hydrothermal calcination process. In this stage, glucose could be transformed into carbon-rich polysaccharides after the hydrothermal treatment, and the following 1200 °C calcination could successfully convert polysaccharides into carbon [29]. In the second part, NiCo$_2$S$_4$ nanostructures were grown on the surface of the carbon shell and the SiO$_2$ core was removed via a hydrothermal treatment method. During the first step, the urea broke down into OH$^-$ and CO$_3$$^{2-}$ under the heating condition and reacted with Co^{2+} and Ni^{2+} to form a Ni–Co precursor on the surface of the carbon shell [30]. Then, in the sulfidation process, the S^{2-} inside the solution replaced OH$^-$ and CO$_3$$^{2-}$; the generation of NiCo$_2S_4$ wrapped the carbon shell accompanied by the formation of NaOH [30, 31]. Next, SiO$_2$ microspheres were etched by the generated NaOH through a hydrolysis reaction, and a hollow spherical structure was formed [31]. When an EMW is transmitted into the composite, such a structure could promote multiple reflections of the wave in the cavity, which is beneficial for consuming more energy.

Fig. 2a displays the XRD patterns of all samples. As for the original SiO$_2$ microsphere, there is a wide peak centered at 22.0°, corresponding to the (101) plane of SiO$_2$ (JCPDS 39-1425) [32]. After the preparation of carbon coating, the center of the broad peak has slightly shifted compared with the pattern of pure SiO$_2$, which could be attributed to the existence of the (002) plane diffraction of carbon at 23.0°, and the new peak located at 43.0° can be indexed to the (100) plane of carbon [26, 33]. To further comprehend the

Fig. 2 **a** XRD patterns and **b** Raman spectra of all samples
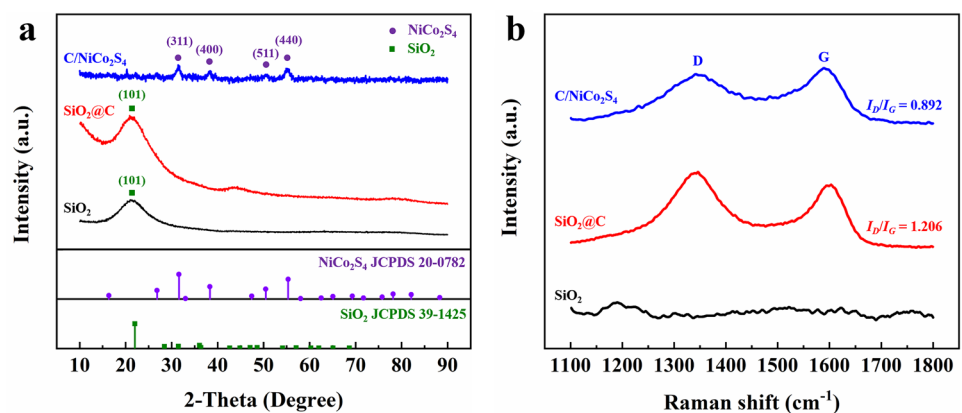
phase composition of the SiO_2@C, HF was used to remove the SiO_2 inside SiO_2@C, and the XRD pattern of the pure carbon shell is shown in Fig. S1. Two significant diffraction peaks centered at about 23.0° and 43.0° could be observed from Fig. S1, further indicating the existence of carbon [26, 33]. After the growth of $NiCo_2S_4$, the peak located at 22.0° disappears, and several new peaks positioned at 31.6°, 38.3°, 50.5°, and 55.3° could be found, which are in good agreement with the diffraction peaks of the (311), (400), (511), and (440) planes of $NiCo_2S_4$ (JCPDS 20-0782) [34, 35]. Besides, the Raman spectra are also collected to have a better understanding of the carbon state, and the spectra of all samples at 1100–1800 cm^{-1} are displayed in Fig. 2b. As for SiO_2, there is no prominent peak except for some fluctuations, demonstrating that there is no carbon or the existence of a very little amount of carbon. For SiO_2@C and C/$NiCo_2S_4$, both samples possess two prominent peaks at 1345 and 1595 cm^{-1}, corresponding to the D and G bands of carbon [36]. Generally, the D band derives from the defects of the carbon lattice and the G band belongs to the stretching vibration of in-plane carbon atoms [37–39]. As a result, the disordered state of carbon could be judged by the intensity ratio of the D peak to G peak (I_D/I_G) and a higher value of I_D/I_G corresponds to a lower graphitization degree and more defects inside the materials [36, 37]. As observed from Fig. 2b, after the introduction of $NiCo_2S_4$, the I_D/I_G value

decreased, meaning improvement of the carbon graphitization degree, which could be assigned to further graphitization during the sulfidation process [40]. Such an interesting phenomenon can be attributed to two factors: (1) the high autogenous pressure inside the autoclave during the hydrothermal process is beneficial to removing the oxygen defects inside the carbon [41], (2) the generation of a small amount of H_2S during the hydrolysis process of Na_2S is reductant, which could promote the graphitization of the carbon [42]. According to the previous research, the defects could play as the centers of polarization and dissipated more energy, leading to a stronger absorption performance [43], meaning that the decrease of defects is not conducive to the improvement of the absorbing performance. However, the number of defects is only one factor that affects the wave-absorbing performance of the material, and other influencing factors will be analyzed in the following part.

XPS measurement is used to characterize the surface elemental states of the products, and the spectra are shown in Fig. 3a. For SiO_2, it can be observed that the sample consists of Si, O, and C, and the weak peak of the C element may be attributed to the specific small amount of impurities. After wrapping the surface with carbon, the C 1s peak is enhanced and the Si 2s and Si 2p peaks become weaker, indicating the existence of carbon on the surface of the SiO_2 microsphere. As for C/$NiCo_2S_4$, several new peaks appear, representing
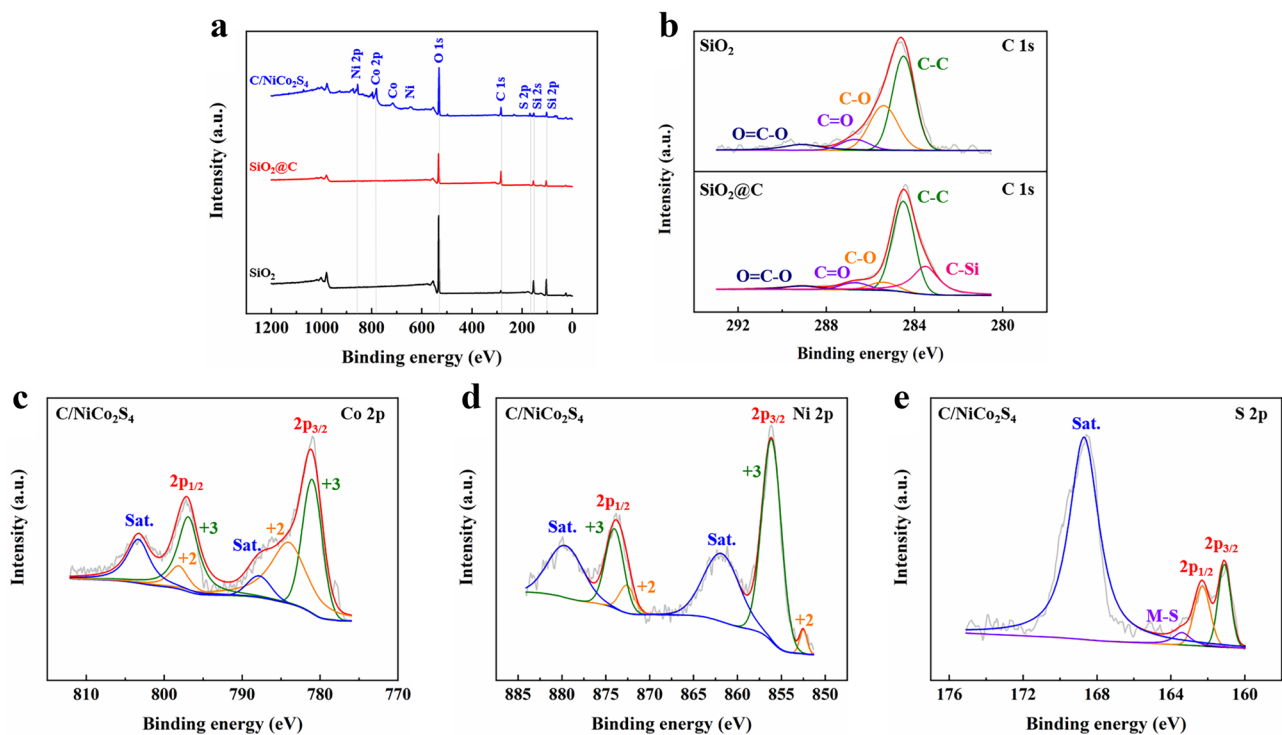

Fig. 3 **a** XPS full spectra of all samples; **b** high-resolution XPS spectra of C 1s for SiO_2 and SiO_2@C; high-resolution XPS spectra of C/$NiCo_2S_4$ composites: **c** Co 2p, **d** Ni 2p, and **e** S 2p

the introduction of Ni, Co, and S. Fig. 3b presents the high-resolution C 1s spectra of SiO_2 and SiO_2@C, and two samples both have four peaks located at 284.5, 285.4, 286.7, and 289.1 eV, corresponding to the C–C, C–O, C=O, and O=C–O bonds [44–46]. Meanwhile, after the fabrication of the carbon coating on the surface of SiO_2, a new peak positioned at 283.7 eV appears, which could be attributed to the presence of the C–Si bond derived from the heterojunction interfaces between the carbon shell and SiO_2 core [47]. The existence of the interfaces can effectively promote the interfacial polarization and improve the wave energy loss capacity of the materials [48]. Fig. 3c–e display the high-resolution XPS spectra of C/$NiCo_2S_4$, and the Gauss fitting method is utilized to analyze the data. In the Co 2p spectrum, the curve is decomposed into six parts and the peaks indexing to Co^{2+} and Co^{3+} can be well fitted with the results of previous research [49, 50]. Analyzing the Ni 2p spectrum by the same method, it can be seen that the curve matches well with the characteristic peak of Ni^{2+} and Ni^{3+} [49]. Fig. 3e presents the spectrum of S 2p, and the binding energy at 161.5 and 162.7 eV could be assigned to S $2p_{1/2}$ and S $2p_{3/2}$, respectively [20, 51]. Besides, the fitted peak located at 163.8 eV could be attributed to the metal-sulfur

(M–S) bonding, such as Ni–S and Co–S bonds [52]. The above results imply the coexistence of Ni^{2+}, Ni^{3+}, Co^{2+}, and Co^{3+}, in keeping with the previous reports on $NiCo_2S_4$ [20, 50].

The morphologies and the microstructures of all samples are shown in Fig. 4. As observed in Fig. 4a, the SiO_2 microsphere possesses a standard spherical structure with a rough surface. After coating with carbon, from Fig. 4b, it can be observed that the carbon shell has a relatively uniform coating on the microsphere and the surface turns from rough to smooth except for the existence of a few pits. Meanwhile, the EDS mappings of SiO_2 and SiO_2@C are shown in Fig. S2, in which it can be seen that the C element is uniformly distributed on all microspheres. As for the C/$NiCo_2S_4$ composite (Fig. 4c, d), $NiCo_2S_4$ nanosheets with a thickness of tens of nanometers are successfully anchored on the carbon shell and wrap the whole carbon shell, forming a loose and porous structure. When an EMW is transmitted to the material, such a structure can effectively reduce the reflection of the wave at the interface between free space and materials, resulting in better impedance matching and improving the absorption performance of the composites [53]. Figure 4e–g show the TEM and HRTEM graphs of C/$NiCo_2S_4$ composites. From Fig. 4e, it could be easily observed

Fig. 4 SEM images of (**a**) SiO_2, (**b**) SiO_2@C, and (**c**, **d**) C/$NiCo_2S_4$; TEM (**e**) and HRTEM (**f**, **g**) images of C/$NiCo_2S_4$; (h1) STEM graph and (h2–h5) elemental mapping of C/$NiCo_2S_4$ composite
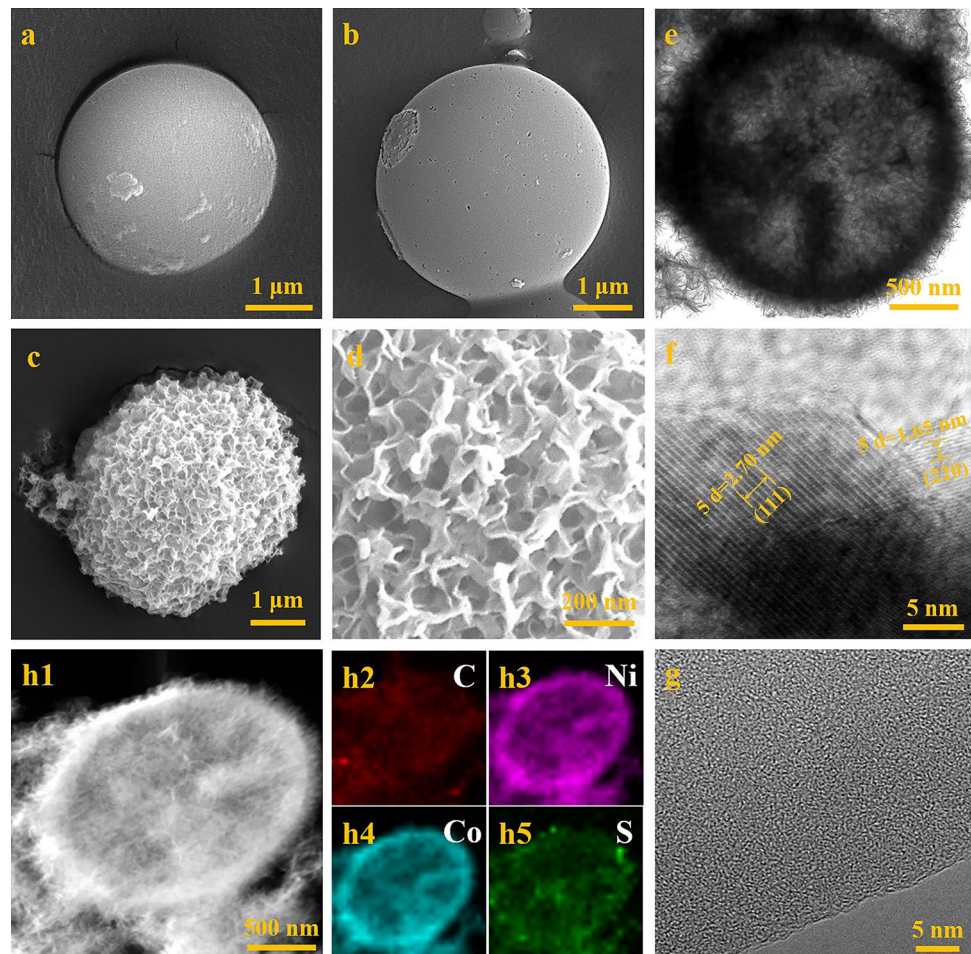
that the center of the sphere is brighter, indicating that the composites have a hollow sphere structure and the thickness of the carbon shell is about 100 nm. Meanwhile, the SEM graph of a defective sample is shown in Fig. S3, and it could be seen that the material possesses a hollow structure, which further proves the above conclusions. Figure 4f, g show the HRTEM images of the samples, and the striation pattern could easily be seen in Fig. 4f, in which spacings are about 0.54 and 0.33 nm, indexing to the (111) and (220) planes of $NiCo_2S_4$ [54, 55]. Meanwhile, the HRTEM graph of carbon is displayed in Fig. 4g, and no clear lattice structure of carbon is found, indicating that the carbon mainly exists in the form of amorphous carbon, in accordance with the Raman analysis. Besides, the EDS mapping images are displayed in Fig. 4h, and it can be seen that the C element is uniformly distributed on the surface of the sphere. Meanwhile, the Ni, Co, and S elements are distributed on the carbon shell more densely and are less positioned at the center of the porous sphere. The above results prove that the $NiCo_2S_4$ nanosheets are wrapped on the shell entirely, corresponding to the observation results through SEM.

The microwave absorption property of the material is evaluated by the RL based on the transmission line theory, and the RL value is calculated by the following equations [37, 56, 57]:

$$RL(dB) = 20\lg\left|\frac{Z_{in} - Z_0}{Z_{in} + Z_0}\right| \qquad (1)$$

$$Z_{in} = Z_0\sqrt{\frac{\mu_r}{\varepsilon_r}}\tanh\left[j\left(\frac{2\pi}{c}\right)fd\sqrt{\mu_r\varepsilon_r}\right] \qquad (2)$$

where Z_{in} and Z_0 represent the input and free space impedance and c and d refer to the speed of light in the vacuum and the thickness of the sample. In general, a lower RL value indicates better absorbing performance, and the bandwidth of the RL value less than −10.00 dB at a specific thickness is named EAB. Fig. 5a–f present the three-dimensional and two-dimensional RL values at different thicknesses and frequency of all samples. For pristine SiO_2, RL_{min} only achieves −3.79 dB with a thickness of 5.00 mm at 8.04 GHz. Next, through cooperation with carbon, the RL_{min} value of $SiO_2@C$ reaches −31.73 dB at 1.73 mm and the EAB achieves 6.02 GHz from 11.98 to 18.00 GHz at 1.85 mm. Then, after the growth of $NiCo_2S_4$, the value of RL_{min} could reach up to −65.10 and −61.13 dB with the matching thickness of 1.56 and 1.77 mm at 16.14 and 13.36 GHz, and the EAB of the sample could further improve to 6.60 GHz (11.40–18.00 GHz) at 1.75 mm, which covers the whole Ku band. Meanwhile, through adjusting the matching thickness, the effective band of $C/NiCo_2S_4$ can reach 14.40 GHz, including the whole C, X, and Ku bands and part of the S band. The microwave absorption property of the hollow carbon sphere is shown in Fig. S4, and the value of RL_{min} is weaker than −10.00 dB, indicating a poor absorption performance. Such a result further proves that the decoration of $NiCo_2S_4$ nanosheets could enhance the microwave absorption performance significantly. Therefore, through our subtle structural design, a microwave absorber with a wide bandwidth and strong absorption performance is realized. Also, the RL_{min} and EAB values of $C/NiCo_2S_4$ are compared with those of some carbon-based composites and transition

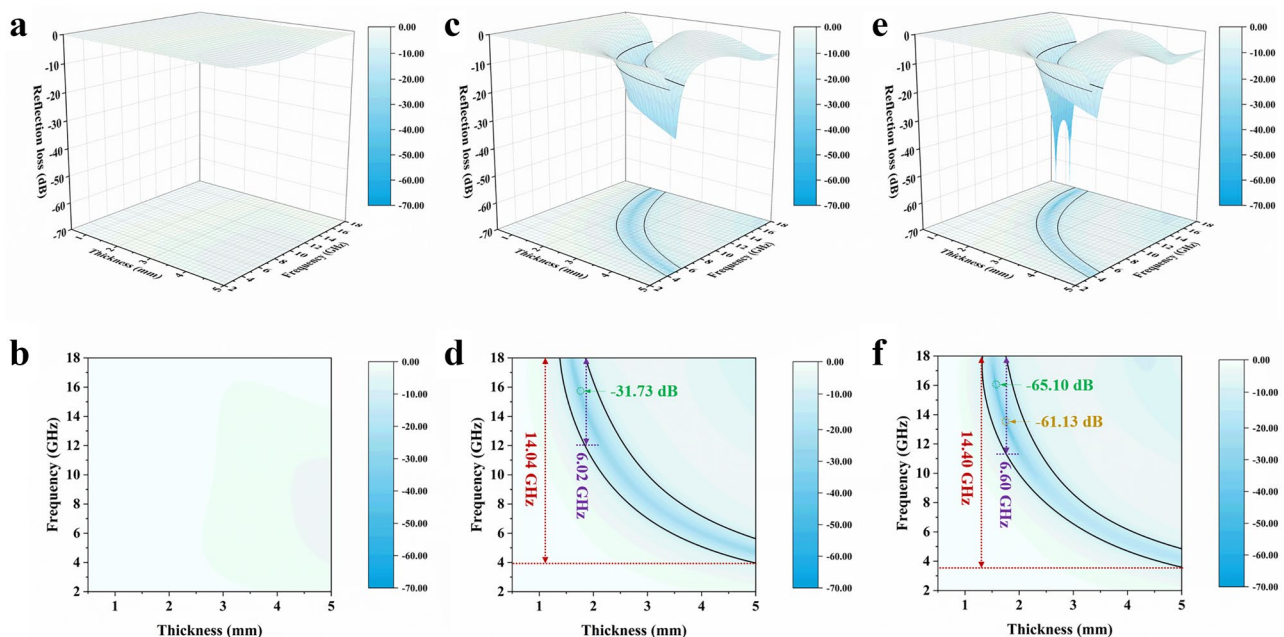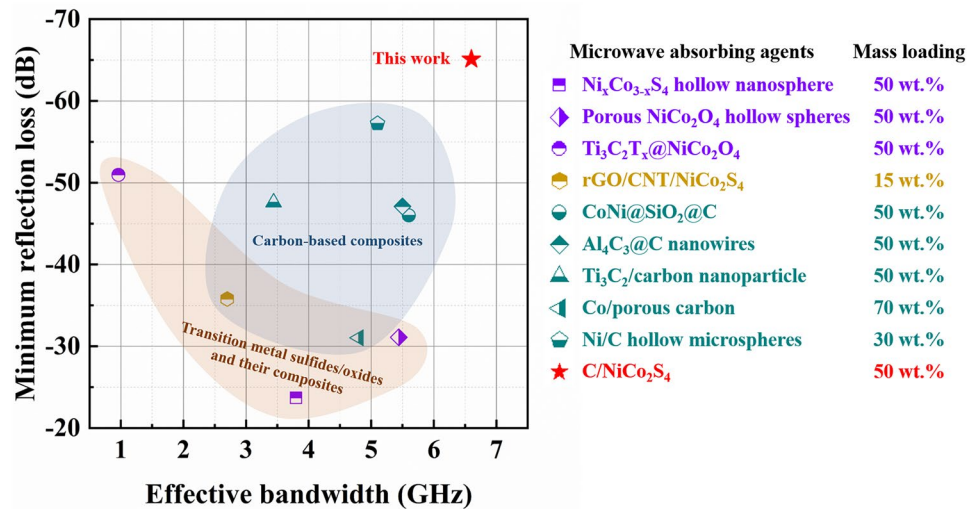**Fig. 5** The three-dimensional and two-dimensional RL maps of **a, d** SiO_2, **b, e** $SiO_2@C$, and **c, f** $C/NiCo_2S_4$

Fig. 6 The RL_{min} and EAB values of the microwave absorbers reported in the previous literature

metal sulfides/oxides and their composites that have been previously reported [18, 23, 58–64]. As shown in Fig. 6 and Table S1, it could be observed that our product possesses strong absorption performance and a wide absorption bandwidth, which can serve as an ideal absorber in the future.

Generally, two important parameters have important influences on the microwave absorption performance of the material: impedance matching and attenuation constant [31]. Impedance matching describes the condition of the interface between free space and material; when the sample has a good impedance matching, the wave transmitted to the surface of the samples will be mostly entering the materials. In contrast, a poor impedance matching will cause the reflection of EMWs at the interface, resulting in a bad absorption performance. The impedance matching of the samples could be evaluated by the absolute value of $Z = Z_{in}/Z_0$; when the value of Z reaches 1, the incident wave could be totally transmitted to the inside of the material, which is beneficial for energy consumption. Figure 7 shows the impedance matching characteristics of the samples, and $SiO_2@C$ and $C/NiCo_2S_4$ possess a larger area close to 1 than SiO_2, indicating a better impedance matching performance. In addition, when the RL value of $C/NiCo_2S_4$

reaches the minimum while the frequency and matching thickness are 16.14 GHz and 1.56 mm, the Z value is approximately equal to 1, proving that the impedance matching is a key factor that dominates the wave absorption performance. As for the hollow carbon shell, the impedance matching data is displayed in Fig. S5, and the largest Z value is less than 0.5; such a result shows that the carbon shell possesses a poor impedance matching, meaning most of the wave is reflected at the surface of the sample and leads to a poor absorption performance, corresponding to the measurement results and theory analysis. As with the attenuation constant, it describes the wave energy loss capacity of materials, and a larger value of the attenuation constant means a stronger dissipation capacity. The calculation of the attenuation constant generally complies with the following formula [65]:

$$\alpha = \frac{\sqrt{2}\pi f}{c}\left[\left(\mu''\varepsilon'' - \mu'\varepsilon'\right) + \sqrt{\left(\mu''\varepsilon'' - \mu'\varepsilon'\right)^2 + \left(\mu'\varepsilon'' + \mu''\varepsilon'\right)^2}\right]^{\frac{1}{2}}$$

(3)

Figure 8 displays the attenuation constant (α) of all samples at 2–18 GHz. The SiO_2 shows the lowest α values of all materials, indicating a poor energy loss capacity. For
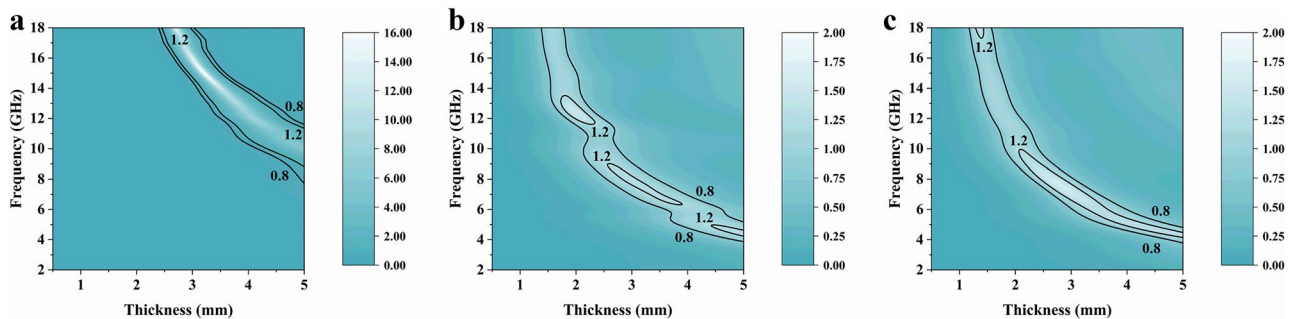

Fig. 7 The impedance matching characteristics of **a** SiO_2, **b** $SiO_2@C$, and **c** $C/NiCo_2S_4$
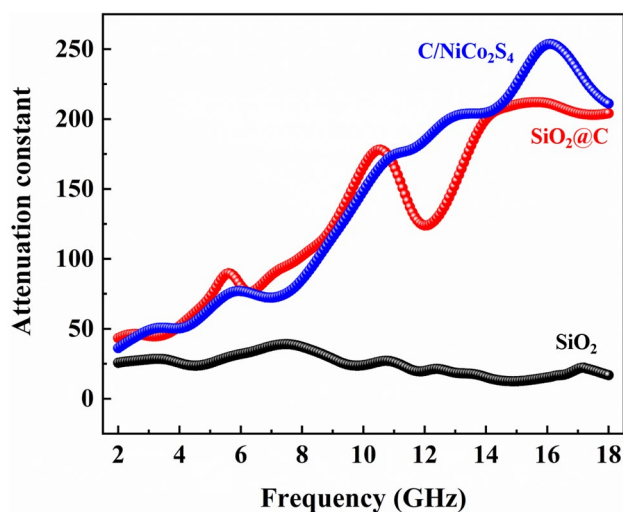
Fig. 8 Attenuation constant of all samples

SiO_2@C and C/$NiCo_2S_4$, at 2–11 GHz, both have similar attenuation constants, and at 11–18 GHz, C/$NiCo_2S_4$ has a larger α value than SiO_2@C. Meanwhile, the α values of SiO_2@C and C/$NiCo_2S_4$ are significantly higher than that of SiO_2, consistent with the data of RL values. Besides, the α value of the hollow carbon shell is displayed in Fig. S6, and it can be found that the sample possesses an ultrahigh attenuation constant, even larger than 1000, indicating a strong wave energy loss capacity. However, the carbon shell only shows a weak absorption performance, which could be attributed to the poor impedance matching. Therefore, through the reasonable design of the structure of the material, the addition of the $NiCo_2S_4$ significantly improved the impedance matching performance, leading to a strong absorption performance of the material.

In order to elucidate the reason of the excellent absorbing property of the material, we analyze the electromagnetic parameters of the samples. Generally, the complex permittivity ($\varepsilon_r = \varepsilon' - j\varepsilon''$) has a vital influence on the dielectric properties of the material, where ε' and ε'' represent the electric field energy storage and loss capacity of the sample [66, 67]. Figure 9 shows the dielectric parameters of the samples. As displayed in Fig. 9a, SiO_2 possesses the lowest ε' values among the three samples, and the ε' curve changes slightly at 2–18 GHz. After wrapping the microsphere with carbon, the ε' of the material markedly improves, and the growth of $NiCo_2S_4$ facilitates the further improvement of ε'. In addition, it could be seen that the ε' values of both SiO_2@C and C/$NiCo_2S_4$ show a declining tendency with increasing frequency, which could be ascribed to the dipole orientation frequency being lower than the alternate frequency of the external electromagnetic field [53]. As for ε'', the ranking of ε'' value of all samples is C/$NiCo_2S_4$ > SiO_2@C > SiO_2. Meanwhile, several resonance peaks derived from the

enhanced polarization due to the formation of new interfaces could be found at 10–18 GHz of C/$NiCo_2S_4$ and SiO_2@C composites, which are beneficial to the energy loss of EMW [8]. The average $\tan\delta_\varepsilon$ value of C/$NiCo_2S_4$ is higher than those of SiO_2@C and SiO_2, demonstrating a stronger dielectric loss. Notably, at 2–10 GHz, C/$NiCo_2S_4$ owns a similar $\tan\delta_\varepsilon$ value as SiO_2@C, and at 11–18 GHz, the $\tan\delta_\varepsilon$ value of C/$NiCo_2S_4$ is higher than that of SiO_2@C, indicating a stronger dielectric loss performance of the material. The variation trend of $\tan\delta_\varepsilon$ is similar to that of the attenuation constant, and such a result proves that the dielectric loss plays a dominant role in energy loss. The dielectric parameters of hollow carbon spheres are shown in Fig. S7, and the sample exhibits a high $\tan\delta_\varepsilon$ value, leading to a strong energy loss capacity, in accordance with the analysis of the attenuation constant. Meanwhile, the carbon shell exhibits exorbitant ε' and ε'' values, which often lead to impedance mismatch, consistent with the above results [17].

Commonly, the dielectric loss mainly originates from conductive loss and polarization loss [6]. Between them, the conductive loss is proportional to the electrical conductivity σ, and according to the free-electron theory, the relation between σ and ε'' can be described as [8]:

$$\sigma \approx 2\pi\varepsilon_0 f\varepsilon'' \tag{4}$$

where ε_0 and f represent the permittivity of the vacuum and frequency of microwave [44]. Therefore, after the fabrication of carbon coating, the conductivity of the material increases, leading to more conductive loss, and C/$NiCo_2S_4$ has a higher conductivity. As for polarization loss which is closely related to the relaxation process, the process could be described by the relationship between ε' and ε'' [68, 69]:

$$\left(\varepsilon' - \frac{\varepsilon_s + \varepsilon_\infty}{2}\right)^2 + \left(\varepsilon''\right)^2 = \left(\frac{\varepsilon_s - \varepsilon_\infty}{2}\right)^2 \tag{5}$$

In this equation, ε_∞ means the dielectric constant at the high-frequency limit and ε_s represents static permittivity and a relaxation process corresponding to a semicircle called Cole-Cole semicircle inside the graph [68, 69]. Figures 9b–d and S8 display the ε'-ε'' curves of all samples, and it can be observed that SiO_2 and SiO_2@C possess 3 and 4 semicircles, indicating that the growth of carbon coating can effectively enhance the polarization relaxation, which could be attributed to the formation of new interfaces. Notably, both C/$NiCo_2S_4$ and the hollow carbon shell possess 5 semicircles, indicating a better relaxation performance. In addition, the improvements of the polarization relaxation can lead to consuming more incident wave energy, resulting in a higher attenuation constant, which matches well with the above results [48].

The magnetic property of the samples is shown in Fig. S9. For all samples, the μ' values are close to 1 and the μ'' values
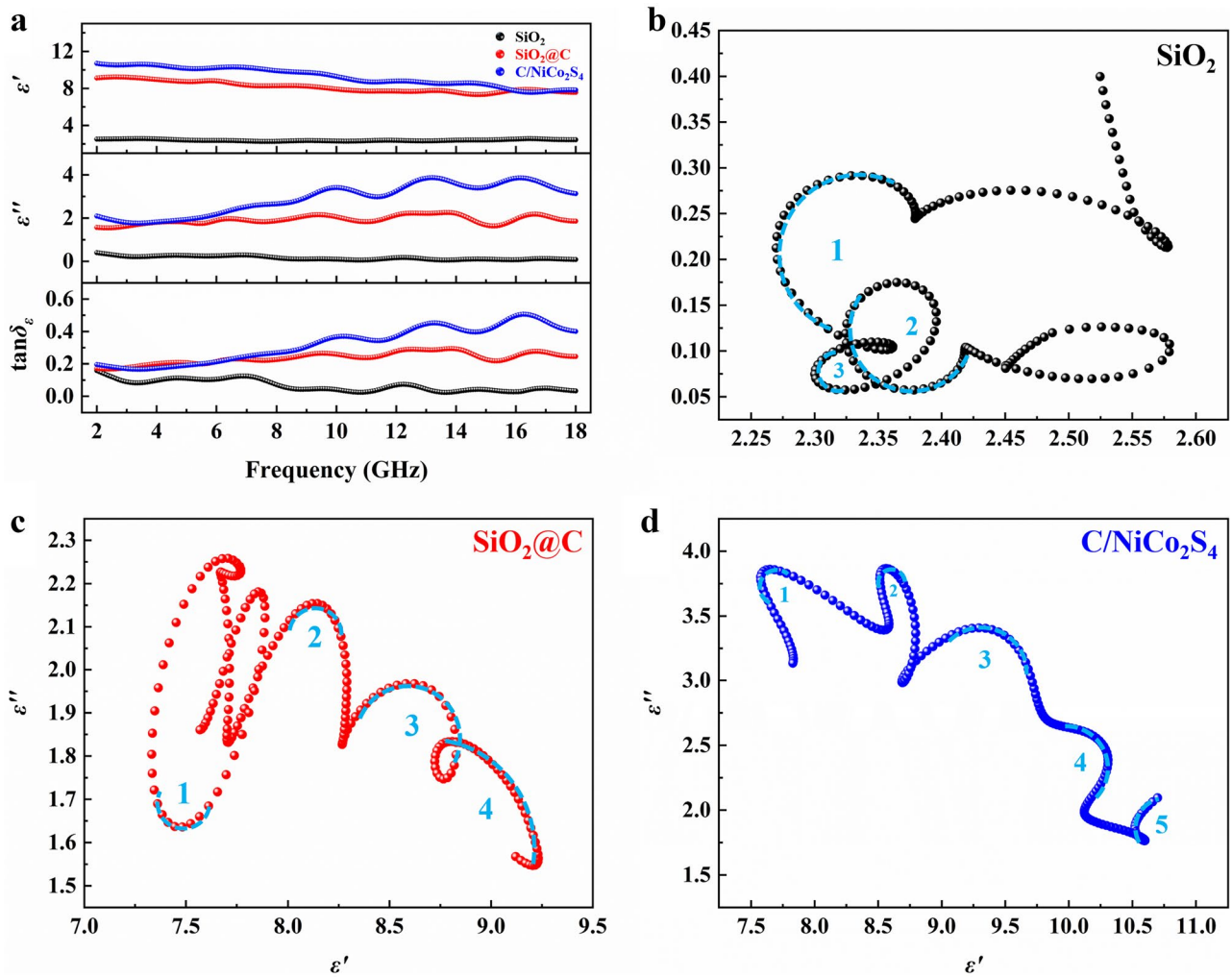
Fig. 9 **a** Dielectric parameters of all samples; Cole-Cole semicircles of **b** SiO$_2$, **c** SiO$_2$@C, and **d** C/NiCo$_2$S$_4$

approach 0, indicating a weak magnetic loss performance. Notably, there is an abnormal phenomenon that the μ'' of some samples reach larger than 0.5 at 2–4 GHz, which could

be illustrated as follows: The surface of the material may scatter the local electric field and redirect the propagating direction of the concomitant magnetic field. In this process,

Fig. 10 Schematic illustration of wave absorption mechanism of C/NiCo$_2$S$_4$
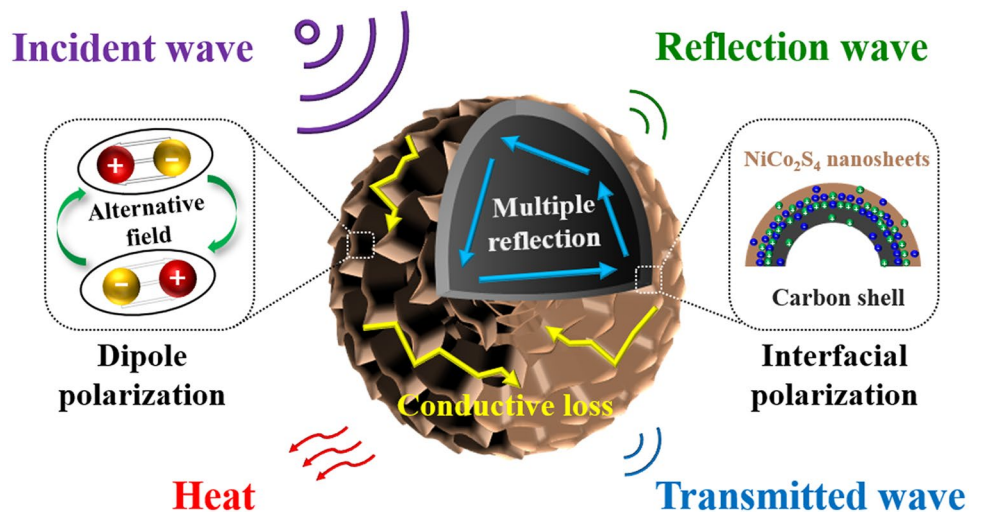
the variational magnetic field could induce electric currents according to Lenz's law, and the generated currents can be consumed by the material, leading to the energy loss of the magnetic field [70]. Meanwhile, it could be seen that after the introduction of $NiCo_2S_4$, the μ' value increases slightly and the μ'' value has no obvious change, indicating that the dielectric loss plays a dominant role in wave energy consumption of $C/NiCo_2S_4$ composites.

Therefore, the EMW absorption mechanisms of $C/NiCo_2S_4$ could be concluded as Fig. 10. When an EMW was transmitted to the surface of $C/NiCo_2S_4$, due to the excellent impedance matching performance, the wave could be propagated into the material, except for being slightly reflected at the interface between the composite and free space [71]. Inside the material, the hollow carbon sphere was considered the template, and the $NiCo_2S_4$ nanosheets construct a connected network, which was beneficial to the conductive loss [72]. Meanwhile, the existence of the defects inside the carbon could act as the center of dipole polarization, and the heterogeneous interface between carbon and the $NiCo_2S_4$ nanosheets could effectively promote the interfacial polarization [68, 73]. Notably, the wave that penetrated into the cavity structure of the hollow carbon sphere can be reflected multiple times and consume energy [74]. During the above processes, much of the EMW energy could be transformed into heat energy, leading to an excellent microwave absorption performance [74].

4 Conclusions

In summary, a facile approach to synthesize a $C/NiCo_2S_4$ composite with a hollow spherical structure is proposed by using SiO_2 microspheres as templates. The composites are synthesized by a low-cost and facile process, and the $NiCo_2S_4$ nanosheets are successfully anchored on the surface of the hollow carbon shell. In addition, the constituents, microstructures, electromagnetic parameters, and microwave absorption performances of the composites are analyzed in detail. After the preparation of carbon coating and the growth of $NiCo_2S_4$, due to the improvements of impedance matching and the attenuation constant, $C/NiCo_2S_4$ shows a superior microwave-absorbing performance, where an RL_{min} below −65.10 dB could be achieved with a relatively thin thickness of 1.56 mm and the EAB reaches 6.60 GHz (11.40–18.00 GHz, covering the whole Ku band) at 1.75 mm. Meanwhile, compared with the other absorbers previously reported, our products possesses an excellent absorbing capacity and a wide effective bandwidth, indicating that the $C/NiCo_2S_4$ composite could serve as an ideal microwave absorber in the future.

Author contribution *Peitao Hu*: Investigation, writing — original draft. *Dong Shun*: Supervision, data curation, writing — review and editing. *Fang Yuan*: Formal analysis. *Xiutao Li*: Formal analysis. *Changqing Hong*: Writing — review and editing, methodology.

Declarations

Conflict of interest The authors declare no competing interests.

References

1. Wu Z, Pei K, Xing L, Yu X, You W, Che R (2019) Enhanced microwave absorption performance from magnetic coupling of magnetic nanoparticles suspended within hierarchically tubular composite. Adv Funct Mater 29:1901448
2. Lan X, Li Y, Wang Z (2020) High-temperature electromagnetic wave absorption, mechanical and thermal insulation properties of in-situ grown SiC on porous SiC skeleton. Chem Eng J 397:125250
3. Jia Y, Sun R, Pan Y, Wang X, Zhai Z, Min Z, Zheng G, Liu C, Shen C, Liu X (2021) Flexible and thin multifunctional waterborne polyurethane/Ag film for high-efficiency electromagnetic interference shielding, electro-thermal and strain sensing performances. Compos Pt B Eng 210:108668
4. Wang C, Wang B, Cao X, Zhao J, Chen L, Shan L, Wang H, Wu G (2021) 3D flower-like Co-based oxide composites with excellent wideband electromagnetic microwave absorption. Compos Pt B Eng 205:108529
5. Cheng H, Pan Y, Chen Q, Che R, Zheng G, Liu C, Shen C, Liu X (2021) Ultrathin flexible poly (vinylidene fluoride)/MXene/silver nanowire film with outstanding specific EMI shielding and high heat dissipation. Adv Compos Hybrid Mat. https://doi.org/10.1007/s42114-021-00224-1
6. Wang J, Cui Y, Wu F, Shah T, Ahmad M, Zhang A, Zhang Q, Zhang B (2020) Core-shell structured Fe/Fe₃O₄@TCNFs@TiO₂ magnetic hybrid nanofibers: preparation and electromagnetic parameters regulation for enhanced microwave absorption. Carbon 165:275–285
7. Cheng JB, Yuan WJ, Zhang AN, Zhao HB, Wang YZ (2020) Porous CoNi nanoalloy@N-doped carbon nanotube composite clusters with ultra-strong microwave absorption at a low filler loading. J Mater Chem C 8:13712–13722
8. Liu P, Gao S, Huang W, Ren J, Yu D, He W (2020) Hybrid zeolite imidazolate framework derived N-implanted carbon polyhedrons with tunable heterogeneous interfaces for strong wideband microwave attenuation. Carbon 159:83–93
9. Deng Z, Li Y, Zhang HB, Zhang Y, Luo JQ, Liu LX, Yu ZZ (2019) Lightweight Fe@C hollow microspheres with tunable cavity for broadband microwave absorption. Compos. Pt B Eng. 177:107346
10. Ni J, Zhan R, Qiu J, Fan J, Dong B, Guo Z (2020) Multi-interfaced graphene aerogel/polydimethylsiloxane metacomposites with tunable electrical conductivity for enhanced electromagnetic interference shielding. J Mater Chem C 8:11748–11759

11. Zhi D, Li T, Li J, Ren H, Meng F (2021) A review of three-dimensional graphene-based aerogels: synthesis, structure and application for microwave absorption. Compos Pt B Eng. 211:108642

12. Song Z, Liu X, Sun X, Li Y, Nie X, Tang W, Yu R, Shui J (2019) Alginate-templated synthesis of CoFe/carbon fiber composite and the effect of hierarchically porous structure on electromagnetic wave absorption performance. Carbon 151:36–45

13. Liu Y, Chen Z, Xie W, Song S, Zhang Y, Dong L (2019) In-situ growth and graphitization synthesis of porous Fe_3O_4/carbon fiber composites derived from biomass as lightweight microwave absorber. ACS Sustain Chem Eng 7:5318–5328

14. Hu Q, Yang R, Mo Z, Lu D, Yang L, He Z, Zhu H, Tang Z, Gui X (2019) Nitrogen-doped and Fe-filled $CNTs/NiCo_2O_4$ porous sponge with tunable microwave absorption performance. Carbon 153:737–744

15. Liu D, Du Y, Xu P, Liu N, Wang Y, Zhao H, Cui L, Han X (2019) Waxberry-like hierarchical Ni@C microspheres with high-performance microwave absorption. J Mater Chem C 7:5037–5046

16. Cui L, Tian C, Tang L, Han X, Wang Y, Liu D, Xu P, Li C, Du Y (2019) Space-confined synthesis of core-shell $BaTiO_3$@carbon microspheres as a high-performance binary dielectric system for microwave absorption. ACS Appl Mater Inter 11:31182–31190

17. Li Q, Zhu J, Wang S, Huang F, Liu Q, Kong X (2020) Microwave absorption on a bare biomass derived holey silica-hybridized carbon absorbent. Carbon 161:639–646

18. Qiu Y, Lin Y, Yang H, Wang L, Wang M, Wen B (2020) Hollow Ni/C microspheres derived from Ni-metal organic framework for electromagnetic wave absorption. Chem Eng J 383:123207

19. Ning M, Man Q, Tan G, Lei Z, Li J, Li RW (2020) Ultrathin MoS_2 nanosheets encapsulated in hollow carbon spheres: a case of a dielectric absorber with optimized impedance for efficient microwave absorption. ACS Appl Mater Inter 12:20785–20796

20. Yuan D, Huang G, Yin D, Wang X, Wang C, Wang L (2017) Metal-organic framework template synthesis of $NiCo_2S_4$@C encapsulated in hollow nitrogen-doped carbon cubes with enhanced electrochemical performance for lithium storage. ACS Appl Mater Inter 9:18178–18186

21. Liu Y, Li Z, Yao L, Chen S, Zhang P, Deng L (2019) Confined growth of $NiCo_2S_4$ nanosheets on carbon flakes derived from eggplant with enhanced performance for asymmetric supercapacitors. Chem Eng J 366:550–559

22. Li Y, An F, Wu H, Zhu S, Lin C, Xia M, Xue K, Zhang D, Lian K (2019) A $NiCo_2S_4$/hierarchical porous carbon for high performance asymmetrical supercapacitor. J Power Sources 427:138–144

23. Zhao T, Hu J, Zhao X, Peng X, Yang W, Tang C, Li T, Ahmad I (2019) Synthesis and electromagnetic wave absorption properties of 3D spherical $NiCo_2S_4$ composites. J Alloy Compd 795:327–335

24. Dong S, Hu P, Li X, Hong C, Zhang X, Han J (2020) $NiCo_2S_4$ nanosheets on 3D wood-derived carbon for microwave absorption. Chem Eng J 398:125588

25. Xu J, Cui Y, Wang J, Fan Y, Shah T, Ahmad M, Zhang Q, Zhang B (2020) Fabrication of wrinkled carbon microspheres and the effect of surface roughness on the microwave absorbing properties. Chem Eng J 401:126027

26. Cheng Y, Zhao H, Zhao Y, Cao J, Zheng J, Ji G (2020) Structure-switchable mesoporous carbon hollow sphere framework toward sensitive microwave response. Carbon 161:870–879

27. Yong Y, Yang Y, Wen X, Jun D (2014) Microwave electromagnetic and absorption properties of magnetite hollow nanostructures. J Appl Phys 115:17A521

28. Song J, Han W, Dong S, Fang C, Cheng Y, Liu D, Zhang X (2020) Constructing hydrothermal carbonization coatings on carbon fibers with controllable thickness for achieving tunable sorption of dyes and oils via a simple heat-treated route. J Colloid Interf Sci 559:263–272

29. Dong S, Zhang W, Zhang X, Hu P, Han J (2018) Designable synthesis of core-shell SiCw@C heterostructures with thickness-dependent electromagnetic wave absorption between the whole X-band and Ku-band. Chem Eng J 354:767–776

30. Sivanantham A, Ganesan P, Shanmugam S (2016) Hierarchical $NiCo_2S_4$ nanowire arrays supported on Ni foam: an efficient and durable bifunctional electrocatalyst for oxygen and hydrogen evolution reactions. Adv Funct Mater 26:4661–4672

31. Xia C, Alshareef HN (2015) Self-templating scheme for the synthesis of nanostructured transition-metal chalcogenide electrodes for capacitive energy storage. Chem Mater 27:4661–4668

32. Li K, Feng S, Jing C, Chen Y, Liu X, Zhang Y, Zhou L (2019) Assembling a double shell on a diatomite skeleton ternary complex with conductive polypyrrole for the enhancement of supercapacitors. Chem Commun 55:13773–13776

33. Tang H, Yan D, Lu T, Pan L (2017) Sulfur-doped carbon spheres with hierarchical micro/mesopores as anode materials for sodium-ion batteries. Electrochim Acta 241:63–72

34. Liu X, Wu Z, Yin Y (2017) Hierarchical $NiCo_2S_4$@PANI core/shell nanowires grown on carbon fiber with enhanced electrochemical performance for hybrid supercapacitors. Chem Eng J 323:330–339

35. Liang K, He W, Deng X, Ma H, Xu X (2018) Controlled synthesis of $NiCo_2S_4$ hollow spheres as high-performance electrode materials for supercapacitors. J Alloy Compd 735:1395–1401

36. Wang L, Huang M, Yu X, You W, Zhang J, Liu X, Wang M, Che R (2021) MOF-derived $Ni_{1-x}Co_x$@carbon with tunable nano-microstructure as lightweight and highly efficient electromagnetic wave absorber. Nanomicro Lett 12:1–17

37. Wang X, Lu Y, Zhu T, Chang S, Wang W (2020) $CoFe_2O_4$/N-doped reduced graphene oxide aerogels for high-performance microwave absorption. Chem Eng J 388:124317

38. Yu Z, Lv X, Mao K, Yang Y, Liu A (2020) Role of in-situ formed free carbon on electromagnetic absorption properties of polymer-derived SiC ceramics. J Adv Ceram 9:617–628

39. Xie P, Liu Y, Feng M, Niu M, Liu C, Wu N, Sui K, Patil RR, Pan D, Guo Z, Fan R (2021) Hierarchically porous Co/C nanocomposites for ultralight high-performance microwave absorption. Adv Compos Hybrid Mat 4:173–185

40. Zheng Y, Wang X, Zhao W, Cao X, Liu J (2018) Phytic acid-assisted synthesis of ultrafine $NiCo_2S_4$ nanoparticles immobilized on reduced graphene oxide as high-performance electrode for hybrid supercapacitors. Chem Eng J 333:603–612

41. Nethravathi C, Rajamathi M (2008) Chemically modified graphene sheets produced by the solvothermal reduction of colloidal dispersions of graphite oxide. Carbon 46:1994–1998

42. Cao A, Liu Z, Chu S, Wu M, Ye Z, Cai Z, Chang Y, Wang S, Gong Q, Liu Y (2010) A facile one-step method to produce graphene-CdS quantum dot nanocomposites as promising optoelectronic materials. Adv Mater 22:103–106

43. Wang H, Meng F, Huang F, Jing C, Li Y, Wei W, Zhou Z (2019) Interface modulating CNTs@PANi hybrids by controlled unzipping of the walls of CNTs to achieve tunable high-performance microwave absorption. ACS Appl Mater Inter 11:12142–12153

44. Chen JP, Jia H, Liu Z, Kong QQ, Hou ZH, Xie LJ, Sun GH, Zhang SC, Chen CM (2020) Construction of C-Si heterojunction interface in SiC whisker/reduced graphene oxide aerogels for improving microwave absorption. Carbon 164:59–68

45. Tang L, Zhang J, Wu C, Tang Y, Ma H, Kong J, Gu J (2021) UV etched random copolymer membrane coated PBO fibers/cyanate ester wave-transparent laminated composite. Compos. Pt B Eng 212:108680

46. Wang Y, Xie W, Liu H, Gu H (2020) Hyperelastic magnetic reduced graphene oxide three-dimensional framework with superb oil and organic solvent adsorption capability. Adv Compos Hybrid Mat 3:473–484

47. Abbas SS, Rees GJ, Kelly NL, Dancer CE, Hanna JV, McNally T (2018) Facile silane functionalization of graphene oxide. Nanoscale 10:16231–16242

48. Xu J, Sun L, Qi X, Wang Z, Fu Q, Pan C (2019) A novel strategy to enhance the multiple interface effect using amorphous carbon packaged hydrogenated TiO_2 for stable and effective microwave absorption. J Mater Chem C 7:6152–6160

49. Xiong X, Waller G, Ding D, Chen D, Rainwater B, Zhao B, Wang Z, Liu M (2015) Controlled synthesis of $NiCo_2S_4$ nanostructured arrays on carbon fiber paper for high-performance pseudocapacitors. Nano Energy 16:71–80

50. Chen Y, Liu T, Zhang L, Yu J (2019) $NiCo_2S_4$ nanotubes anchored 3D nitrogen-doped graphene framework as electrode material with enhanced performance for asymmetric supercapacitors. ACS Sustain Chem Eng 7:11157–11165

51. Xu R, Lin J, Wu J, Huang M, Fan L, He X, Wang Y, Xu Z (2017) A two-step hydrothermal synthesis approach to synthesize $NiCo_2S_4$/NiS hollow nanospheres for high-performance asymmetric supercapacitors. Appl Surf Sci 422:597–606

52. Wang P, Li C, Dong S, Ge X, Zhang P, Miao X, Wang R, Zhang Z, Yin L (2019) Hierarchical $NiCo_2S_4$@NiO core-shell heterostructures as catalytic cathode for long-life LiO_2 batteries. Adv Energy Mater 9:900788

53. Hu P, Dong S, Li X, Chen J, Hu P (2020) Flower-like $NiCo_2S_4$ microspheres based on nanosheet self-assembly anchored on 3D biomass-derived carbon for efficient microwave absorption. ACS Sustain Chem Eng 8:10230–10241

54. Fan YM, Liu Y, Liu X, Liu Y, Fan LZ (2017) Hierarchical porous $NiCo_2S_4$-rGO composites for high-performance supercapacitors. Electrochim Acta 249:1–8

55. Dong M, Wang Z, Yan G, Wang J, Guo H, Li X (2020) Confine growth of $NiCo_2S_4$ nanoneedles in graphene framework toward high-performance asymmetric supercapacitor. J Alloy Compd 822:153645

56. Ye X, Chen Z, Ai S, Hou B, Zhang J, Liang X, Zhou Q, Liu H, Cui S (2019) Porous SiC/melamine-derived carbon foam frameworks with excellent electromagnetic wave absorbing capacity. J Adv Ceram 8:479–488

57. Lu X, Zhu D, Li X, Li M, Chen Q, Qing Y (2021) Gelatin-derived N-doped hybrid carbon nanospheres with an adjustable porous structure for enhanced electromagnetic wave absorption. Adv Compos Hybrid Mat. https://doi.org/10.1007/s42114-021-00258-5

58. Jia Z, Wang B, Feng A, Liu J, Zhang C, Zhang M, Wu G (2019) Fabrication of $Ni_xCo_{3-x}S_4$ hollow nanosphere as wideband electromagnetic absorber at thin matched thickness. Ceram Int 45:15854–15859

59. Wang L, Guan Y, Qiu X, Zhu H, Pan S, Yu M, Zhang Q (2017) Efficient ferrite/Co/porous carbon microwave absorbing material based on ferrite@metal-organic framework. Chem Eng J 326:945–955

60. Qin M, Zhang L, H Wu (2020) Dual-template hydrothermal synthesis of multi-channel porous $NiCo_2O_4$ hollow spheres as high-performance electromagnetic wave absorber. Appl Surf Sci 515:146132

61. Zhou S, Huang Y, Liu X, Yan J, Feng X (2018) Synthesis and microwave absorption enhancement of CoNi@SiO_2@C hierarchical structures. Ind Eng Chem Res 57:5507–5516

62. Hua A, Li Y, Pan D, Luan J, Wang Y, He J, Tang S, Geng D, Ma S, Liu W, Zhang Z (2020) Enhanced wideband microwave absorption of hollow carbon nanowires derived from a template of Al_4C_3@C nanowires. Carbon 161:252–258

63. Zhu W, Ye F, Li M, Wang X, Zhou Q, Fan X, Xue J, Li X (2020) In-situ growth of wafer-like Ti_3C_2/Carbon nanoparticle hybrids with excellent tunable electromagnetic absorption performance. Compos Pt B Eng 202:108408

64. Hou T, Wang B, Ma M, Feng A, Huang Z, Zhang Y, Jia Z, Tan G, Cao H, Wu G (2020) Preparation of two-dimensional titanium carbide ($Ti_3C_2T_x$) and $NiCo_2O_4$ composites to achieve excellent microwave absorption properties. Compos Pt B Eng 180:107577

65. Wang Y, Li X, Han X, Xu P, Cui L, Zhao H, Liu D, Wang F, Du Y (2020) Ternary Mo_2C/Co/C composites with enhanced electromagnetic waves absorption. Chem Eng J 387:12415

66. Wang Y, Gao X, Fu Y, Wu X, Wang Q, Zhang W, Luo C (2019) Enhanced microwave absorption performances of polyaniline/graphene aerogel by covalent bonding. Compos Pt B Eng 169:221–228

67. Liu P, Gao S, Wang Y, Zhou F, Huang Y, Luo J (2020) Metal-organic polymer coordination materials derived Co/N-doped porous carbon composites for frequency-selective microwave absorption. Compos Pt B Eng 202:108406

68. Liu P, Zhu C, Gao S, Guan C, Huang Y, He W (2020) N-doped porous carbon nanoplates embedded with CoS_2 vertically anchored on carbon cloths for flexible and ultrahigh microwave absorption. Carbon 163:348–359

69. Zhao H, Cheng Y, Zhang Z, Yu J, Zheng J, Zhou M, Zhou L, Zhang B, Ji G (2020) Rational design of core-shell Co@C nanotubes towards lightweight and high-efficiency microwave absorption. Compos Pt B Eng 196:108119

70. Zhou X, Jia Z, Feng A, Wang X, Liu J, Zhang M, Wu G (2019) Synthesis of fish skin-derived 3D carbon foams with broadened bandwidth and excellent electromagnetic wave absorption performance. Carbon 152:827–836

71. Wen B, Yang H, Lin Y, Ma L, Qiu Y, Hu F (2021) Controlling the heterogeneous interfaces of S, Co co-doped porous carbon nanosheets for enhancing the electromagnetic wave absorption. J Colloid Interf Sci 586:208–218

72. Li M, Fan X, Xu H, Ye F, Xue J, Li X, Cheng L (2020) Controllable synthesis of mesoporous carbon hollow microsphere twined by CNT for enhanced microwave absorption performance. J Mater Sci Technol 59:164–172

73. Wang R, Qi X, Xie R, Gong X, Deng C, Zhong W (2020) Constructing heterostructural Fe@Fe_3C@carbon nanotubes/reduced graphene oxide nanocomposites as lightweight and high-efficiency microwave absorbers. J Mater Chem C 8:14515–14522

74. Li X, Li M, Lu X, Zhu W, Xu H, Xue J, Ye F, Liu Y, Fan X, Cheng L (2021) A sheath-core shaped ZrO_2-SiC/SiO_2 fiber felt with continuously distributed SiC for broad-band electromagnetic absorption. Chem Eng J 419:129414